Efficient and flexible characterization of paleokarst seismic signatures using point-spread function-based convolution modeling

Kristian Jensen and Isabelle Lecomte, University of Bergen; Xavier Janson, Bureau of Economic Geology, University of Texas at Austin; Jan Tveranger, NORCE Norwegian Research Centre AS*

Summary

Paleokarst reservoirs originate from collapse, degradation and infill of karstified rock, and typically feature spatially heterogeneous elements such as breakdown products, sediment infills and preserved open cavities on all scales. Seismic characterization of paleokarst reservoirs therefore remains a challenging task. Through the application of 2(3)D spatial convolution operators, referred to as point-spread functions, efficient and flexible seismic modeling of prestack depth migrated paleokarst signatures may be obtained at a low computational cost. The present paper investigates the application of this method on paleokarst-type reservoirs by performing a qualitative comparison of seismic signatures generated using this approach and signatures obtained from a physical modeling experiment. We further illustrate the suitability/utility of the method by analyzing modeled prestack depth-migrated images of a selected target area in a 3D geocellular model of the Devil's Sinkhole in Texas.

Introduction

The process of degradation of karst to form paleokarst normally produces very complex structures and contrasting petrophysical properties on many scales. Some features of the initial karst system can be preserved, such as open cavities or old sediment fills, whereas others parts can be filled in by cements or have collapsed entirely; forming sags, vertical faults and breccia pipes affecting the overburden (Loucks, 1999). A significant proportion of the elements and heterogeneities characterizing paleokarst are generally well below seismic resolution.

A recent study by Wang *et al*. (2019) illustrates the challenges associated with obtaining proper quality and resolution of seismic images of a paleokarst system in the Tarim Basin, China. The authors emphasize the importance of high acquisition density, wide-azimuth coverage and small image bins for achieving proper sampling and obtaining sufficient resolution. Given these acquisition requirements and the complexity of the structures, full-waveform modeling and migration of seismic data for assessing paleokarst signatures in 3D models is computationally expensive. Efficient and flexible seismic modeling methods for characterizing seismic paleokarst signatures are therefore attractive.

In the following, we apply 3D convolution modeling via 3D target-oriented spatial convolution operators referred to as *point-spread functions* (*PSFs*; Lecomte *et al.*, 1998; Lecomte, 2008) for simulating prestack depth-migrated (PSDM) images (Lecomte *et al.*, 2003). The PSF-based convolution modeling accounts for 3D resolution effects due to specific acquisition geometries, frequency-band limitations, incidence-angle variation, and propagation effects (e.g. limited illumination) in the overburden. The computational cost of this method is comparable to 1D convolution as employed by the industry. We here perform a validation of using the method on paleokarst reservoirs by 1) conducting a qualitative comparison with signatures obtained by Xu *et al*. (2016) from a physical model of simple cave geometries, and 2) employing the method on a 3D geocellular model of Devil's Sinkhole (Janson and Fomel, 2011) to demonstrate its applicability to paleokarst geology.

Method: PSF-based convolution modelling (PSDM)

The PSF can be obtained by Fourier Transform (FT) of a *PSDM filter* defined in the wavenumber domain (Lecomte, 2008; Figure 1).

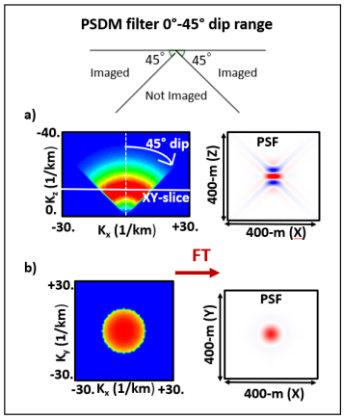

Figure 1: 2D cross-sections of a 3D PSDM filter and corresponding PSF for a 20-Hz dominant frequency (Ricker wavelet), an average Vp of 3 km/s, 0˚-incidence (null-offset), and an illumination range of 0˚- 45˚ in geological dip. (a) vertical cross-section (XZ). (b) horizontal cross-section (XY).

The PSDM filter represents the dip-range of reflectors potentially imaged at a selected location, as any reflector perpendicular to the covered wavenumber spectrum would appear on the image in that zone. Furthermore, the extension of the wavenumber spectrum defines the overall resolution

of both reflectors and diffraction points. The corresponding PSF is, in essence, a 3D convolution operator which, when applied to an input reflectivity grid, yields a simulated PSDM image. PSDM filters may be estimated by various ray-based approaches (Lecomte, 2008), but full-waveform generated PSFs may also be applied (e.g. Xie *et al*., 2005; Toxopeus *et al*., 2010). A simpler alternative is to analytically calculate the PSDM filter with just a few parameters, i.e., wavelet, average P-wave velocity (Vp), incident angle, and illuminated-dip range (Lecomte *et al*., 2016), as illustrated in Figure 1.

Case 1: comparison with physical modeling experiment

The validation of PSF-based convolution modeling carried out here is inspired by Xu *et al*. (2016), who employed a physical modelling experiment to assess paleokarst signatures termed *String Beads Responses* (*SBRs*; Figure 2 (left)). We used a synthetic model similar to the physical model used by Xu *et al*. (2016). We also performed 1D convolution modeling, in order to highlight the limitations of this approach.

Lacking a full 3D model, a 2.5D-model was generated based on a vertical cross-section illustrated in Xu *et al*. (2016). Vp and density values of the layers were set identical to those used by Xu *et al.*, (2016). S-velocity was defined as half of the Vp-value, which is a reasonable Vp/Vs relation estimate for carbonate rocks (Anselmetti and Eberli, 1997). Vs was set to zero in the water layer. We used six target models, representing six cave configurations (Figure 2 (center)). The depth of the structures was set identical to depths used by Xu *et al*. (2016). Cave infill velocity was set to Vp = 5 km/s and Vs = 2.5 km/s, corresponding to high-velocity infill values used by Xu *et al.* (2016). Density was set to 2.65 g/cm^3 for the entire model A 3D survey-acquisition geometry derived from Xu *et al*. (2016) was designed, and a 25-Hz zero-phased Ricker wavelet was selected (same dominant frequency as in the physical modeling of Xu *et al*. (2016)). Finally, as the background medium of the layer in which the caves are embedded has a Vp of 6 km/s, this value was chosen as input for the PSDM-filter.

Illumination coverage of the target area (the depth of the modeled caves) was estimated by ray tracing, using a wavefront-construction approach introduced by Vinje *et al*. (1993). For simplicity's sake, only zero-offset ray-paths to the target area are shown in Figure 2 (right). The resulting illumination suggested a proper geological-dip range to be set to 0°-45°. A PSF was generated and convolved with the reflectivity grids generated for the six target scenarios. 1D convolution was also performed on the reflectivity grids using the same wavelet. The target areas of the velocity models, the PSF convolution results, and the 1D convolution results, all in the XZ-plane, are illustrated in Figure 2 (center). Note that seismic data is often automatically plotted with a smoothing filter to enhance the visual aesthetics of the images. We have, however, omitted such filtering in this case in order to highlight the contrast between the outcome of a 2D PSF-based convolution versus that of a repeated-1D one, for which such artificial smoothing introduces a false non-physical lateral resolution effect.

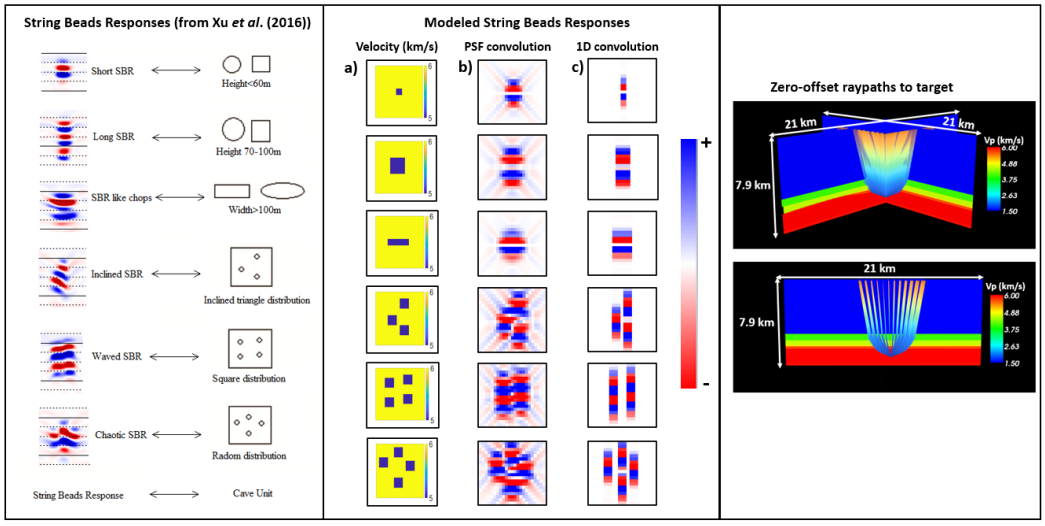

Figure 2: (left) Classification of six primary categories of SBRs. Image courtesy of Xu *et al*. (2016, p. B40). (center) (a) P-velocity models for the six target areas in the XZ-plane. (b-c) Seismic signatures obtained after PSF convolution modeling and 1D convolution (**NB!** No "cosmetic smoothing" in display has been applied to (b) and (c) to better preserve the actual - and false - response of a 1D convolution, the latter having per-definition a 1-pixel width whatever the original grid sampling is). (right) Zero-offset survey-to-target ray-paths in synthetic background model.

DOI:10.1190/segam2020-3426595.1

Lacking detailed information about the exact processing and migration parameters applied by Xu *et al.* (2016), results can only be compared qualitatively. Furthermore, as we only extracted a 2.5D-model of a 2D slice provided in Xu *et al*. (2016), instead of generating an exact replica in 3D, some mismatches can be expected. However, by accounting for both lateral resolution and lack of illumination of walls steeper than 45°, we see from Figure 2 (center) that the seismic signatures obtained via PSF-based convolution modeling more closely resemble the responses obtained by Xu *et al.* (2016). Due to lateral resolution effects, the seismic signatures are smeared horizontally. In contrast, we see that the cavities in the 1D convolution case are automatically separated horizontally as neither lateral resolution nor limited illumination of steep walls is considered. This is particularly evident for the so-called "Inclined", "Waved", and "Chaotic" SBRs.

Case 2: Devil's Sinkhole, Texas

The Devil's Sinkhole is a vertical cavern with an asymmetric hourglass shape located in the Edwards Limestone, Texas (Neubert *et al*., 2008). A 3D geocellular model containing a layered overburden and the sinkhole itself was generated on a regular rectangular grid of resolution 6m × 6m × 2m and populated with velocity- and density values from an initial facies-populated 3D grid (Janson and Fomel, 2011).

In order to demonstrate the use of PSF convolution modeling on an actual paleokarst structure, we analyzed the modeled seismic responses from two different versions of the Janson and Fomel (2011) model. Both versions have identical background, but employ different cavity fill; one consisting of breccia, the other consisting of silt. The Vp model with breccia infill is illustrated in Figure 3, with selected target area highlighted.

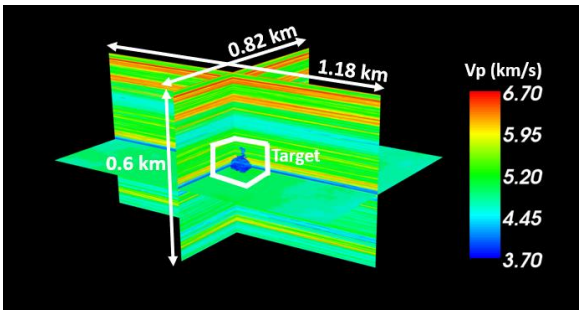

Figure 3: P-velocity model of Devil's Sinkhole, Texas, with breccia infill in the sinkhole. The depth slice at z = 0.35 km is displayed.

We performed PSF-based convolution modeling on both models using two PSFs: one with illumination down to 45˚ dip, as a proxy for standard 3D seismic, and one down to 20˚ dip to specifically emphasize the impact of limited illumination on seismic images. The latter could be caused by features such as complex structures in the overburden (salt bodies, etc.) or simply be due to a thin high-velocity layer above the target (Eide *et al*., 2018). The dip ranges correspond well to standard values obtained from wide-azimuth versus narrow-azimuth acquisition (Feng *et al*., 2012; Wang *et al*., 2019). For illustration, we also modeled with a perfect illumination scenario (90° dip) while superimposing the actual cave shape on top of this figure. A comparison with modeled post-stack migrated results obtained by Janson and Fomel (2011) for the same target area was carried out. Their procedure involved first convolving the reflectivity grid generated from the velocity and density grids with a 30-Hz Ricker wavelet, and then applying an exploding-reflector algorithm using split-step Fourier wavelet propagation (Kessinger, 1992). Finally, Janson and Fomel (2011) performed a depth-domain reverse split-step Fourier migration using a smooth version of the velocity model. Similar to Jason and Fomel (2011), we employed a 30-Hz Ricker wavelet for all PSF-based convolution modeling. Background velocity was set to 5 km/s based on average Vp values in the target area. Seismic results obtained in the XZ-plane are shown in Figure 4; results obtained in the XY-plane are displayed in Figure 5.

Looking at the results, the level of detail at the top of the sinkhole (Figure 4) varies between the four models, especially for the silt cases. The level of resolution obtained by employing the exploding reflector and split-step Fourier algorithm is slightly better than that obtained using PSF convolution modeling of 45° dip, thus indicating an illumination of slightly above 45° for this case. This is indicated in the part of the seismic data outlined by the white squares in Figure 4. By comparing the breccia and silt cases in both planes, we further see that the silt-filled cavities, as expected, stand out as brighter spots, due to the higher impedance contrast. Furthermore, lateral resolution is impacted by reduction in illumination (45° versus 20° dip). The sinkhole cavity appears increasingly smeared and the level of detail decreases as illumination coverage drops. Compare for instance the results obtained by all modeling results to the actual cave shape highlighted in the perfect illumination plots. On all seismic data, both the vertical and lateral extent of the sinkhole appears to be far larger than the actual cave shape. Thus, with limited illumination coverage, there is a risk of misjudging the spatial extent of the sinkhole. This effect is exacerbated by the lack of illumination of the steep walls of the sinkhole (thus not visible even if having a reflectivity). In reservoir exploration, such effects are crucial to assess.

10.1190/segam2020-3426595.1

Conclusions

Point-spread functions (PSFs) applied as spatial convolution operators allow efficient and flexible modelling of seismic signatures (PSDM) of complex paleokarst reservoirs. Comparison with a physical modeling study shows that, as paleokarst signatures computed via PSFs account for both limited illumination and resolution effects, more realistic signatures are obtained than what may be obtained through conventional 1D convolution, yet at a similar cost. Applying the method to a 3D geocellular model of the Devil's Sinkhole also showed that the PSF-based convolution modelling may be a useful supplement to other modeling approaches for assessing paleokarst signatures affected by variations in illumination coverage and cave infill. However, future studies should venture to verify the method's validity compared to full-waveform approaches, in particular due to the complexity in paleokarst reservoirs.

Acknowledgments

The first author wishes to thank the University of Bergen for PhD-project funding, and thank Fulbright Norway and The Meltzer Research Fund for supporting a four-month stay at Bureau of Economic Geology, University of Texas at Austin in Prof. Sergey Fomel's research group. The first author also thanks The Meltzer Research Fund for additional traveling funds. The authors gratefully acknowledge NORSAR Innovation AS for providing an academic license for their modeling software. Finally, the authors would like to thank the Research Council of Norway for financial support through project #26763/E30 (FOPAK).

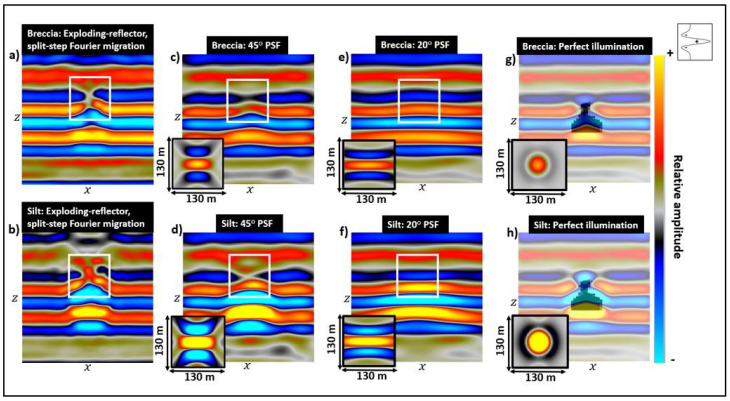

Figure 4: Seismic data generated in the XZ-plane at the target defined in Figure 3. The target area is located at y = 0.5 km, and spans from x = 0.38 – 0.72 km, and from z = 0.14 – 0.48 km. For each result, the PSF is illustrated and scaled in accordance with the seismic data dimensions. The dark shape on (g) and (h) outlines the actual cave shape.

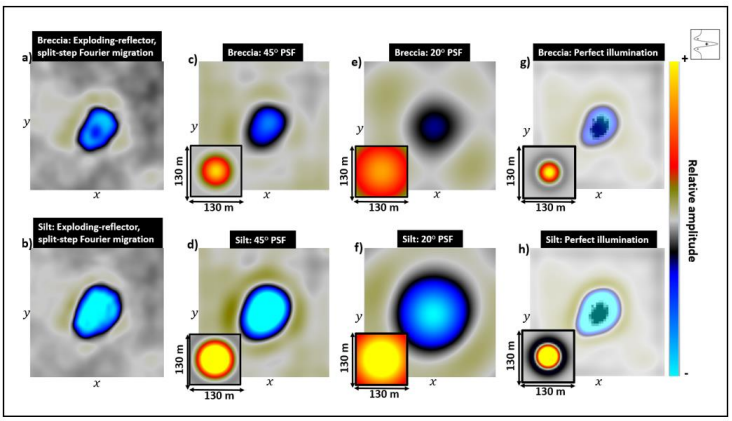

Figure 5: Seismic data generated in the XY-plane at the target defined in Figure 3. The target area is located at z = 0.306 km, and spans from x = 0.38 – 0.72 km, and from y = 0.33 – 0.67 km. For each result, the PSF is illustrated and scaled in accordance with the seismic data dimensions. The dark shape on (g) and (h) outlines the actual cave shape.

REFERENCES

Anselmetti, F. S., and G. P. Eberli, 1997, Sonic velocity in carbonate sediments and rocks, *in* F. J. Marfurt and A. Palaz, eds., Carbonate seismology: SEG, Geophysical Developments Series, **6**, 53–74.

Eide, C. H., N. Schofield, I. Lecomte, S. J. Buckley, and J. A. Howell, 2018, Seismic interpretation of sill complexes in sedimentary basins: implications for the sub-sill imaging problem: Journal of the Geological Society, **175**, 193–209, doi: https://doi.org/10.1144/jgs2017-096.

Feng, X., Y. Wang, X. Wang, N. Wang, G. Gao, and X. Zhu, 2012, The application of high-resolution 3D seismic acquisition techniques for carbonate reservoir characterization in China: The Leading Edge, **31**, 168–179, doi: https://doi.org/10.1190/1.3686914.

Janson, X., and S. Fomel, 2011, 3-D forward seismic model of an outcrop-based geocellular model, *in* O. Martinsen, A. J. Pulham, P. D. Haughton, and M. D. Sullivan, eds., Outcrops revitalized: Tools, techniques and applications: SEPM concepts in sedimentology and paleontology No. 10: SEPM Society for Sedimentary Geology, 87–106.

Kessinger, W., 1992, Extended split-step Fourier migration: 62nd Annual International Meeting, SEG, Expanded Abstracts, 917–920, doi: https://doi.org/10.1190/1.1822254.

Lecomte, I., 2008, Resolution and illumination analyses in PSDM: A ray-based approach: The Leading Edge, **27**, 650–663, doi: https://doi.org/10.1190/1.2919584.

Lecomte, I., and L.-J. Gelius, 1998, Have a look at the resolution of prestack depth migration for any model, survey and wavefields: 68th Annual International Meeting, SEG, Expanded Abstracts, 1112–1115, doi: https://doi.org/10.1190/1.1820082.

Lecomte, I., H. Gjøystdal, and Å. Drottning, 2003, Simulated prestack local imaging: a robust and efficient interpretation tool to control illumination, resolution, and time-lapse properties of reservoirs: 73rd Annual International Meeting, SEG, Expanded Abstracts, 1525–1528, doi: https://doi.org/10.1190/1.1817585.

Lecomte, I., P. L. Lavadera, C. Botter, I. Anell, S. J. Buckley, C. H. Eide, A. Grippa, V. Mascolo, and S. Kjoberg, 2016, 2D convolution modelling of complex geological targets — beyond 1D convolution: First Break, **34**, 99–107.

Loucks, R. G., 1999, Paleocave carbonate reservoirs: Origins, burial-depth modifications, spatial complexity, and reservoir implications: AAPG Bulletin, **83**, 1795–1834.

Neubert, B., J. A. Bellian, X. Xu, K. McGowan, G. M. Schindel, and E. C. Alexander, Jr., 2008, 3-D photo real modeling of Devil's Sinkhole in Rocksprings, Texas: 11th Multidisciplinary Conference on Sinkholes and the Engineering and Environmental Impacts of karst, 188–201.

Toxopeus, G., and J. Thorbecke, 2010, A brief summary of Hessian based modelling in a shared earth environment: 72nd Conference and Exhibition, EAGE, Extended Abstracts, P591, doi: https://doi.org/10.3997/2214-4609.201401319.

Vinje, V., E. Iversen, and H. Gjøystdal, 1993, Traveltime and amplitude estimation using wavefront construction: Geophysics, **58**, 1157–1166, doi: https://doi.org/10.1190/1.1443499.

Wang, N., X.-B. Xie, M. Duan, D. Li, and R.-S. Wu, 2019, Improving seismic image resolution in a carbonate fracture region: A case study: 89th Annual International Meeting, SEG, Expanded Abstracts, 32–36, doi: https://doi.org/10.1190/segam2019-3215909.1.

Xie, X.-B., R.-S. Wu, M. Fehler, and L. Huang, 2005, Seismic resolution and illumination: A wave-equation based analysis: 75th Annual International Meeting, SEG, Expanded Abstracts, 1862–1865, doi: https://doi.org/10.1190/1.2148066.

Xu, C., B. Di, and J. Wei, 2019, A physical modeling study of seismic features of karst cave reservoirs in the Tarim Basin, China: Geophysics, **81**, no. 1, B31–B41, doi: https://doi.org/10.1190/geo2014-0548.1.